
DIFFVOLUME: DIFFUSION MODELS FOR VOLUME GENERATION IN LIMIT ORDER BOOKS

Zhuohan Wang

Department of Informatics
King's College London
London, United Kingdom
zhuohan.wang@kcl.ac.uk

Carmine Ventre

Department of Informatics
King's College London
London, United Kingdom
carmine.ventre@kcl.ac.uk

ABSTRACT

Modeling limit order books (LOBs) dynamics is a fundamental problem in market microstructure research. In particular, generating high-dimensional volume snapshots with strong temporal and liquidity-dependent patterns remains a challenging task, despite recent work exploring the application of Generative Adversarial Networks to LOBs. In this work, we propose a conditional **Diffusion** model for the generation of future LOB **Volume** snapshots (**DiffVolume**). We evaluate our model across three axes: (1) *Realism*, where we show that DiffVolume, conditioned on past volume history and time of day, better reproduces statistical properties such as marginal distribution, spatial correlation, and autocorrelation decay; (2) *Counterfactual generation*, allowing for controllable generation under hypothetical liquidity scenarios by additionally conditioning on a target future liquidity profile; and (3) *Downstream prediction*, where we show that the synthetic counterfactual data from our model improves the performance of future liquidity forecasting models. Together, these results suggest that DiffVolume provides a powerful and flexible framework for realistic and controllable LOB volume generation.

Keywords Limit order books, Volume Generation, Diffusion models

1 Introduction

Limit order books (LOBs) are the backbone of modern financial markets, capturing real-time information on pending buy and sell orders at various price levels Gould et al. [2013]. Among the core components of LOBs, order volume at different price levels serves as a crucial indicator of market liquidity, price discovery, and trading opportunities. Accurate modeling of LOB volumes enables practitioners and researchers to improve trading strategies, optimize market making, and conduct robust market impact analyses Bouchaud et al. [2018]. Therefore, the task of volume generation is fundamental for both theoretical insights and practical financial applications.

Most prior research focuses primarily on event-level generation, with the objective of simultaneously generating price and volume information, which often leads to less accurate and realistic results Li et al. [2020], Coletta et al. [2021], Nagy et al. [2023]. In particular, recent work by Cont et al. [2023] applies Generative Adversarial Networks (GANs) to LOB modeling but only considers six price levels of a single big tick stock. Moreover, GAN-based models are prone to training instability and mode collapse, which can significantly impair their ability to replicate complex volume patterns across time and depth. Therefore, there remains a clear need for advanced modeling techniques that address these limitations in a comprehensive way.

To address these limitations, we introduce **DiffVolume**, a diffusion model-based framework specifically designed for the generation of future LOB volume snapshots. The proposed framework offers three main contributions:

- (1) We develop a novel diffusion model architecture conditioning on past volume trajectories and time of day, which captures the spatial correlation structures and intricate temporal dependencies presented in LOB volume data;

- (2) By additionally conditioning on a target future liquidity profile, we implement counterfactual generation under hypothetical liquidity scenarios;
- (3) We demonstrate the quality and practical utility of the generated data by (i) evaluating the distribution of its data points vis-a-vis the original dataset; and (ii) showing how a downstream liquidity prediction task can be solved more effectively.

2 Related Work

We will discuss related research in three parts.

Limit Order Book Dynamics. The dynamics of LOBs have been extensively studied through various modeling approaches. Poisson processes models treat order arrivals and cancellations as independent events, characterized by a constant or time-varying intensity, providing a simplified representation of order flows Bauwens and Hautsch [2009]. Hawkes processes models extend this framework by incorporating self-exciting properties, effectively modeling the clustering of order events, and capturing the feedback loops inherent in market activity Bacry et al. [2015], Filimonov and Sornette [2012]. Agent-based models simulate the interactions of heterogeneous traders with distinct strategies, allowing a detailed analysis of market microstructure phenomena and emergent behaviors such as volatility clustering and market crashes Paddrik et al. [2012], Byrd et al. [2019], Amrouni et al. [2021], Balch et al. [2019].

Generative Modeling of Limit Order Books. Generative modeling of LOBs can be primarily classified into two categories: autoregressive models and GANs. Autoregressive models generate LOB data sequentially, leveraging previous historical data points to predict future order book states. Hultin et al. [2023] propose a model based on recurrent neural networks (RNNs) that decomposes the joint distribution of LOB transitions into conditional probabilities over order type, price, size, and time delay, each modeled with a dedicated RNN. Similarly, Nagy et al. [2023] present an end-to-end autoregressive model using structured state-space models, which tokenizes message streams and generates realistic LOB transitions. GAN-based models, on the other hand, employ adversarial training to generate realistic synthetic limit order books. Li et al. [2020] introduce Stock-GAN, a conditional Wasserstein GAN designed to generate realistic stock market order streams by capturing historical dependence and mimicking auction mechanisms. Coletta et al. [2021] propose a Conditional GAN framework that reacts to current market states and allows agent interaction within a simulation, showing enhanced realism and responsiveness. Meanwhile, Cont et al. [2023] develop a GAN framework that arguably learns the conditional distribution of future LOB volume states, capturing both stylized facts and some market impact patterns. However, their model can only be applied on large tick stock and limited price levels that are often asymmetric between the two sides of the book. DiffVolume accurately models the volume dynamics across many price levels for both bids and asks, no matter the tick size.

Diffusion Models Theory. The foundational idea of diffusion models is inspired by thermodynamic diffusion Sohl-Dickstein et al. [2015], which proposes to train generative models by adding Gaussian noise over multiple steps and learning to reverse the process. Ho et al. [2020] are the first to propose the Denoising Diffusion Probabilistic Model. Their method involves adding noise in a forward process and denoising in a reverse process to generate high-quality images. Subsequent work focuses on improving sampling quality and training efficiency Nichol and Dhariwal [2021], Song et al. [2021a]. Diffusion models are also closely related to score-based generative modeling, where the model learns the gradient of the data density through denoising score matching Vincent [2011], Song and Ermon [2019]. This connection has been formally unified under the stochastic differential equation framework by Song et al. [2021b]. Recent advances further clarify and optimize the design space of diffusion models under this unified view. For example, Karras et al. [2022] analyze the score matching and noise schedules in depth, leading to improvements in sample quality and generation speed. This line of work provides the theoretical foundation for applying diffusion models to structured data domains such as financial data Koa et al. [2023], Wang and Ventre [2024].

3 Methodology

In this section, we will briefly summarize conditional denoising diffusion probabilistic models from the score-based perspective and describe the proposed DiffVolume architecture in detail.

3.1 Generative Diffusion Models

Denoising Diffusion Probabilistic Models. Denoising Diffusion Probabilistic Models (DDPMs) Sohl-Dickstein et al. [2015], Ho et al. [2020], Luo [2022], Chan et al. [2024] consist of two complementary stochastic processes, a forward (noising) process and a reverse (generative) process. In the forward process, Gaussian noise is progressively added

to the data through a fixed Markov chain, transforming it into a nearly pure noise distribution. The reverse process learns to invert this transformation by iteratively denoising the corrupted data, thereby recovering samples from the data distribution via learned transitions.

Consider a noise strength sequence $0 < \beta_1 < \beta_2 < \dots < \beta_N < 1$ and forward noising process $p(\mathbf{x}_i|\mathbf{x}_{i-1}) = \mathcal{N}(\mathbf{x}_i|\sqrt{1-\beta_i}\mathbf{x}_{i-1}, \beta_i\mathbf{I})$. With $\alpha_i := \prod_{j=1}^i(1-\beta_j)$, we have $p_{\alpha_i}(\mathbf{x}_i|\mathbf{x}_0) = \mathcal{N}(\mathbf{x}_i|\sqrt{\alpha_i}\mathbf{x}_0, (1-\alpha_i)\mathbf{I})$, and the perturbed data distribution is given by $p_{\alpha_i}(\tilde{\mathbf{x}}) = \int p_{\text{data}}(\mathbf{x})p_{\alpha_i}(\tilde{\mathbf{x}}|\mathbf{x})d\mathbf{x}$. The noise scale is predetermined to approximately satisfy $p_{\alpha_N}(\tilde{\mathbf{x}}) \sim \mathcal{N}(\tilde{\mathbf{x}}|\mathbf{0}, \mathbf{I})$, i.e., the terminal distribution is nearly independent of p_{data} . The reverse denoising process can be written as $p_\theta(\mathbf{x}_{i-1}|\mathbf{x}_i) = \mathcal{N}(\mathbf{x}_{i-1}|\frac{1}{\sqrt{1-\beta_i}}(\mathbf{x}_i + \beta_i\mathbf{s}_\theta(\mathbf{x}_i, i)), \beta_i\mathbf{I})$, where $\mathbf{s}_\theta(\mathbf{x}_i, i)$ is called the *score* Song and Ermon [2019]. The training objective is a sum of local denoising score-matching objectives, i.e., finding θ^* that minimizes

$$\sum_{i=1}^N(1-\alpha_i)\mathbb{E}_{p_{\text{data}}(\mathbf{x})}\mathbb{E}_{p_{\alpha_i}(\tilde{\mathbf{x}}|\mathbf{x})}[\|\mathbf{s}_\theta(\tilde{\mathbf{x}}, i) - \nabla_{\tilde{\mathbf{x}}}\log p_{\alpha_i}(\tilde{\mathbf{x}}|\mathbf{x})\|_2^2]. \quad (1)$$

DDPMs and Stochastic Differential Equations. Song et al. [2021b] demonstrate that DDPMs can be understood from the perspective of stochastic differential equations (SDEs). Let $\{\mathbf{x}(t)\}_{t=0}^T$ be a stochastic diffusion process indexed by a continuous time variable $t \in [0, T]$, evolving from $\mathbf{x}(0) \sim p_0$, the true data distribution, to $\mathbf{x}(T) \sim p_T$, approximately the tractable prior distribution. Denote the probability density function of $\mathbf{x}(t)$ by $p_t(\mathbf{x})$ and the transition kernel from $\mathbf{x}(s)$ to $\mathbf{x}(t)$ by $p_{st}(\mathbf{x}(t)|\mathbf{x}(s))$, for $0 \leq s < t \leq T$. Then, we can use an SDE to represent such a forward diffusion process:

$$d\mathbf{x} = \mathbf{f}(\mathbf{x}, t) dt + g(t) d\mathbf{w}, \quad (2)$$

where $\mathbf{f}(\mathbf{x}, t)dt$ is referred to as the *drift* term, and $g(t)d\mathbf{w}$ is referred to as the *diffusion* term. Here, \mathbf{w} is a standard Wiener process and $d\mathbf{w} \sim \mathcal{N}(0, dt\mathbf{I})$. The synthetic data generation process is the reverse process of Eq. (2), which is also an SDE Anderson [1982]:

$$d\mathbf{x} = [\mathbf{f}(\mathbf{x}, t) - g^2(t)\nabla_{\mathbf{x}}\log p_t(\mathbf{x})] dt + g(t) d\bar{\mathbf{w}}, \quad (3)$$

where $\bar{\mathbf{w}}$ is a reverse-time Wiener process and $\nabla_{\mathbf{x}}\log p_t(\mathbf{x})$ is the score of the marginal distribution corresponding to each t . It starts from an initial noise sample $\mathbf{x}(T) \sim p_T$ and gradually denoises it step by step following Eq. (3). Theoretically, if $T \rightarrow \infty$, we obtain $\mathbf{x}(0) \sim p_0$. To estimate $\nabla_{\mathbf{x}}\log p_t(\mathbf{x})$, the score network $\mathbf{s}_\theta(\mathbf{x}, t)$ is trained using the objective function

$$\kappa(t)\mathbb{E}_t\mathbb{E}_{\mathbf{x}(0)}\mathbb{E}_{\mathbf{x}(t)|\mathbf{x}(0)}[\|\mathbf{s}_\theta(\mathbf{x}(t), t) - \nabla_{\mathbf{x}(t)}\log p_{0t}(\mathbf{x}(t)|\mathbf{x}(0))\|_2^2], \quad (4)$$

where $\kappa: [0, T] \rightarrow \mathbb{R}^+$ is a positive weight and $t \sim \mathcal{U}[0, T]$. Eq. (4) is a continuous generalization of Eq. (1). Typically, the continuous form of the DDPM forward process is chosen to be

$$d\mathbf{x} = -\frac{\beta(t)}{2}\mathbf{x} dt + \sqrt{\beta(t)} d\mathbf{w}, \quad (5)$$

i.e., $\mathbf{f}(\mathbf{x}, t) = -\frac{\beta(t)}{2}\mathbf{x}$ and $g(t) = \sqrt{\beta(t)}$. Substituting $\mathbf{f}(\mathbf{x}, t)$ and $g(t)$ in (3), we can get the backward process in SDE form for DDPM.

Conditional DDPMs. How do we inject the conditioning \mathbf{c} into the training and sampling process? Here we follow the *classifier-free guidance* approach Ho and Salimans [2021], combining the conditional and unconditional models as follows:

$$\nabla_{\mathbf{x}}\log \tilde{p}(\mathbf{x}|\mathbf{c}) = \omega\nabla_{\mathbf{x}}\log p(\mathbf{x}|\mathbf{c}) + (1-\omega)\nabla_{\mathbf{x}}\log p(\mathbf{x}), \quad (6)$$

where $\nabla_{\mathbf{x}}\log p(\mathbf{x}|\mathbf{c})$ represents the conditional and $\nabla_{\mathbf{x}}\log p(\mathbf{x})$ represents the unconditional score, corresponding to the conditional and unconditional model distributions. Eq. (6) reduces to the unconditional score when $\omega = 0$, or recovers the conditional score when $\omega = 1$.

3.2 DiffVolume Architecture

DiffVolume is a conditional score-based diffusion model designed to estimate the score function $\mathbf{s}_\theta(\mathbf{x}(t), t, \mathbf{c})$. The architecture is shown in Figure 1. At each diffusion step t , the model takes as input a noised volume snapshot denoted by $\mathbf{x}(t)$. The architecture incorporates two embeddings *price level embeddings* \mathbf{v} , *time step embeddings* t , and an external *conditioning context* \mathbf{c} , which includes variables such as past volume trajectories, time of day and target future liquidity (if applicable). Details on the construction of \mathbf{v} and t are provided below, while the structure of \mathbf{c} is described in Subsection 4.3.

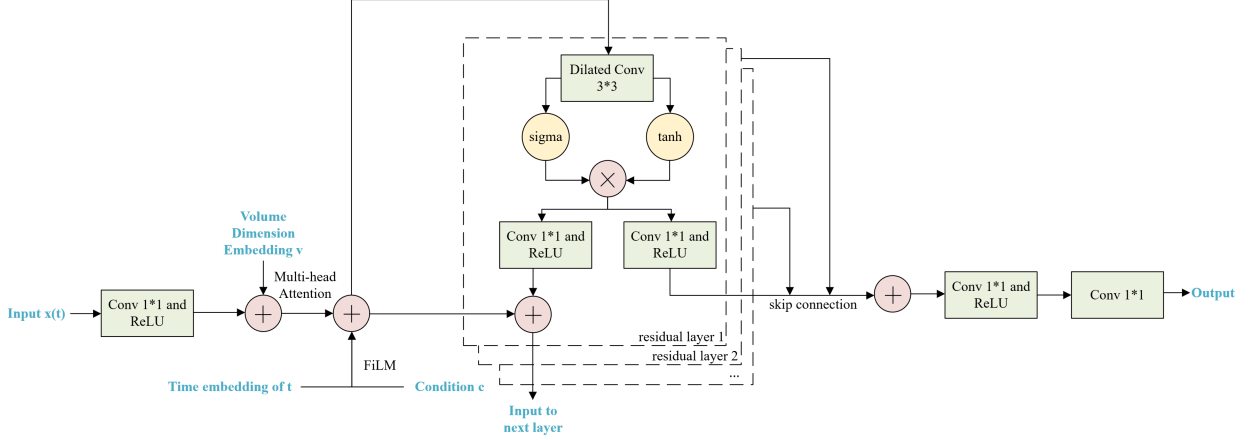


Figure 1: Illustration of DiffVolume Architecture.

The input $x(t)$ is first processed by a 1×1 convolutional layer followed by a ReLU activation. This projects the corrupted volume vector into a higher-dimensional latent feature space, making it more suitable for capturing complex interactions. The resulting latent feature is then augmented with learnable *price level embeddings* \mathbf{v} , where each discrete price level index is mapped to a continuous dense vector. These embeddings enable the model to distinguish between spatially different price levels in the order book. To capture the dependencies across price levels, the combined input is passed through a multi-head self-attention module Vaswani et al. [2017].

To encode the diffusion step t , we adopt a sinusoidal embedding scheme followed by a two-layer MLP with SiLU activations. To incorporate the conditioning information from both t and c , we adopt the Feature-wise Linear Modulation (FiLM) mechanism Perez et al. [2018]. Specifically, the FiLM layers learn affine transformations (scaling and shifting) applied to the intermediate features, parameterized by functions of t and c . This allows the model to adjust its internal computations dynamically, enabling more flexible and adaptive generation.

The core of the DiffVolume architecture is a stack of 32 residual convolutional layers, inspired by WaveNet-style dilated convolutions van den Oord et al. [2016]. Each residual block begins with a dilated 3×3 convolutional layer, which increases the receptive field without increasing model depth. The output is split into two branches: one activated with a \tanh function, and the other with a sigmoid function. The two activations are combined through element-wise multiplication, forming a *soft gating mechanism* that allows the network to selectively pass or suppress signals.

The gated output is then passed through two 1×1 convolutional layers, each followed by a ReLU activation. A residual connection is added between the input and output of each block, facilitating gradient flow and stability during training. In addition, each residual layer outputs a skip connection, which is accumulated across all layers and routed to the final output head. The aggregated skip connections are combined and passed through a final output sequence: a 1×1 convolution followed by ReLU activation, and another 1×1 convolution to produce the final prediction.

This novel architecture enables the model to integrate fine-grained spatial dependencies within each price level and broader contextual signals across the book and conditioning inputs, allowing it to accurately model the high-dimensional structure of LOB volume trajectories.

4 Experimental Setup

In this section, we provide details on the dataset used in our experiments, the preprocessing steps applied to the raw data, as well as the training and sampling procedures.

4.1 Data

We use the LOBSTER data¹ as our LOB data source Huang and Polak [2011]. The platform provides Level-3 data, allowing for a full-fidelity reconstruction of the LOB dynamics. For each day, the dataset contains a message file, which consists of orders sent to an exchange (primarily market, limit, and (partial) cancellation orders), and a snapshot file, which includes the corresponding order book states. To construct our dataset, we sample one snapshot per second

¹<https://lobsterdata.com/>

from the snapshot files. Each snapshot includes the top 10 levels on both the bid and ask sides, resulting in a volume representation of shape $[20, 1]$ per time step.

In particular, we train, evaluate, and test our model separately on four stocks, which are MU (Micron, big tick stock), AAPL (Apple, medium tick stock), ADBE (Adobe, small tick stock) and ZM (Zoom, small tick stock). Stocks are classified as big, medium, or small tick size according to how their tick size compares to the typical bid-ask spread. Variations in tick size can affect bid-ask spreads, order book depth, and execution costs, thus shaping the strategies of market participants and the dynamics of price formation Briola et al. [2025]. For each stock, we use 16 consecutive trading days for training (1 February to 23 February 2023), 1 day for validation (24 February 2023), and the final 2 days for testing (27-28 February 2023).

4.2 Preprocessing

To mitigate the non-stationary behavior typically observed in limit order books—particularly around market open and close—we exclude the first and last 30 minutes of each continuous trading session from our analysis. As a result, we retain only snapshots from the 5.5-hour interval between 10:00 AM and 3:30 PM each day. To ensure data quality and prevent computational inconsistencies, we remove all snapshots with missing values. Given that such instances are extremely rare, their exclusion has a negligible effect on the overall statistical properties of the dataset. Setting the sampling frequency to 1 second results in $\sim 310k$ order book snapshots for training, $\sim 20k$ snapshots for validation, and $\sim 40k$ snapshots for testing.

To mitigate the impact of extreme outliers in volume data, we apply a clipping procedure that caps volume values at the 99th percentile for each price level. This enhances model stability and ensures that learning is not dominated by rare but disproportionately large volume observations. We also adopt a square-root-based normalization scheme as shown in Eq. (7). It is coupled with a scaling constant, to stabilize the input distribution and make the training process more effective:

$$x_{normalized} = \frac{\sqrt{x}}{const}, \quad (7)$$

where $const = 15$ during real training.

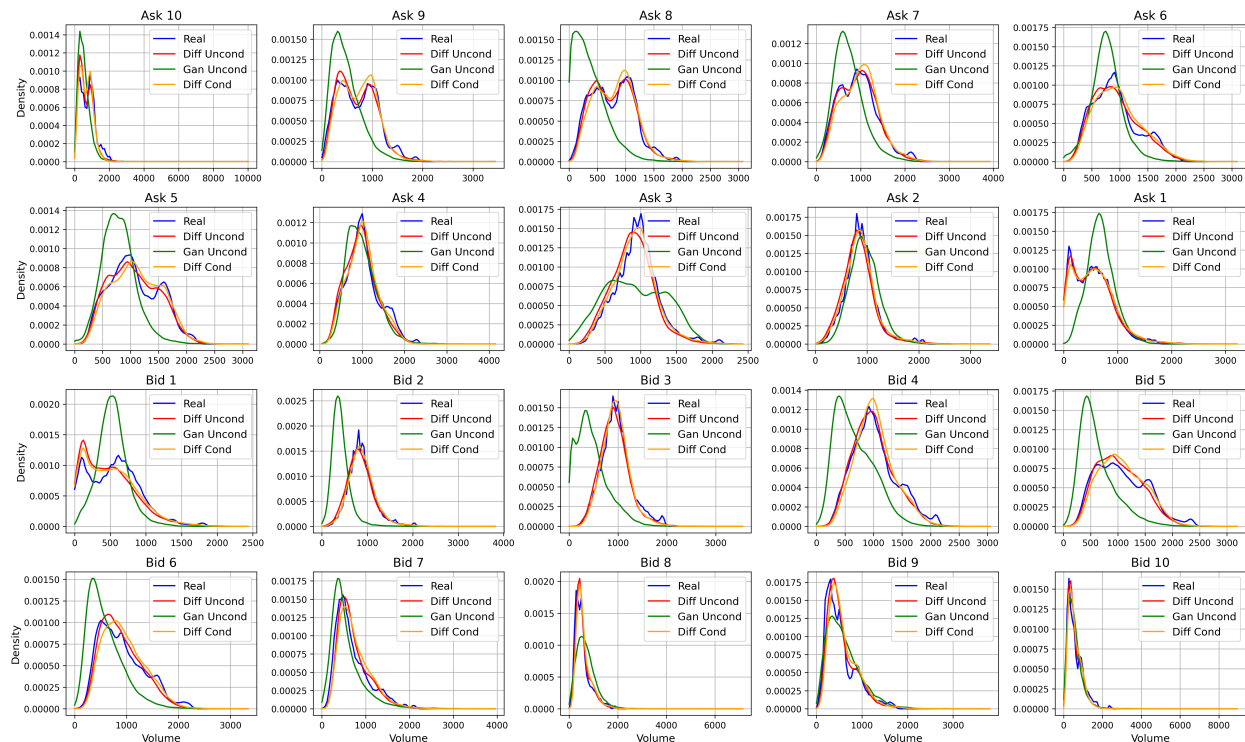


Figure 2: Marginal Volume Distribution.

4.3 Training and Sampling

We consider the task of modeling the conditional distribution of future LOB volume snapshots given multiple conditioning variables. Let $\mathbf{x}_{(t-L+1:t)} \in \mathbb{R}^{L \times D}$ denote the sequence of past volume snapshots over L time steps, where each vector $\mathbf{x}_{(i)} \in \mathbb{R}^D$ represents volume across D price levels (20 levels in our case) and $x_{(i)}^j$ represents the volume value at the j -th price level in time step i . Our objective is to generate a realistic sequence of future volumes $\mathbf{x}_{(t+1:t+L)} \in \mathbb{R}^{L \times D}$ based on a *conditioning context* \mathbf{c} , which includes the past volume trajectory $\mathbf{x}_{(t-L+1:t)}$, the time of day $\tau_{(t+1:t+L)}$ and, in counterfactual settings, the future liquidity indicator $\lambda_{(t+1:t+L)}$. The length L is set to 32 in the training and sampling stage.

The time of day $\tau_{(t+1:t+L)}$ is constructed as a normalized scalar ratio reflecting the elapsed time since the market opening, calculated as

$$\tau_{(i)} = \frac{\Delta t_i}{T_{total}}, \quad \text{for } i \in \{t+1, \dots, t+L\}, \quad (8)$$

where Δt_i is the number of seconds elapsed from the start of the trading session, and $T_{total} = 19800$ seconds denotes the total trading duration (5.5 hours). The resulting sequence $\tau_{(t+1:t+L)} \in \mathbb{R}^{L \times 1}$ serves as a continuous temporal encoding aligned with each future snapshot. By conditioning on the time of the day, we provide temporal context that captures non-stationary behaviors over intraday horizons.

The future liquidity indicator λ provides a coarse but informative signal reflecting the expected market depth over the prediction horizon. Each value in λ is calculated as the sum of the volume of the corresponding LOB snapshot:

$$\lambda_{(i)} = \sum_{j=1}^D x_{(i)}^j, \quad \text{for } i \in \{t+1, \dots, t+L\}. \quad (9)$$

Conditioning the model on this sequence, we enable controlled generation, allowing the model to produce volume patterns that not only exhibit realistic microstructure dynamics but also align with target liquidity profiles.

To effectively train the conditional diffusion model and prevent overfitting or instability, we adopt the early stopping Goodfellow et al. [2016] and exponential moving average (EMA) mechanism of the network weights Nichol and Dhariwal [2021]. Early stopping is used based on the validation loss, where training is terminated if the validation loss does not improve by at least 0.001 over a patience window of 100 epochs. EMA parameters are updated after each optimization step as $\theta_{EMA} \leftarrow \alpha \cdot \theta_{EMA} + (1 - \alpha) \cdot \theta$, where $\alpha = 0.999$. We train the model using Adam optimizer Kingma and Ba [2015] with a learning rate of 1×10^{-4} and a batch size of 64. We adopt the ancestral sampling procedure Ho et al. [2020], a widely used method in DDPMs, to generate LOB volume snapshots.

5 Experimental Results

In this section, we address three key research questions. (1) To what extent do the generated samples exhibit statistical fidelity to real-world limit order book data? (2) Can DiffVolume generate meaningful counterfactual samples in response to varying liquidity conditions? (3) Are the counterfactually generated samples informative enough to support downstream applications, such as future liquidity prediction?

5.1 Realism

We begin by assessing the realism of the generated LOB volumes from different models, focusing on their ability to replicate key statistical properties observed in real market data. We compare four sources of volume data: (i) the empirical testing dataset (*Real*), (ii) diffusion model without future liquidity condition (*Diff Uncond*), (iii) WGAN-GP model without future liquidity condition (*GAN Uncond*), and (iv) diffusion model with future liquidity condition (*Diff Cond*). To ensure a fair comparison of generative quality, we primarily focus on *GAN Uncond* and *Diff Uncond*, where no strong future information is provided during training. The *Diff Cond* model, although conditioned on future liquidity profiles, is included here for completeness, as it plays a key role in later sections and shows promise for future applications. We will take MU as an illustrative example for our plots and summarize the performance for the four stocks in Table 1.

Marginal Volume Distributions. Figure 2 presents kernel density estimates of marginal volume distributions at each price level. Real LOB volumes exhibit multi-modal and heavy-tailed characteristics. GAN-generated samples fail to reproduce these higher-order statistics, often yielding overly smooth unimodal distributions. Both *Diff Uncond* and *Diff Cond* accurately capture the skewness and kurtosis of empirical data, outperforming *GAN Uncond*.

	MU			AAPL			ADBE			ZM		
	Wasserstein	KL	KS	Wasserstein	KL	KS	Wasserstein	KL	KS	Wasserstein	KL	KS
Diff Uncond	40.34	0.256	0.091	165.783	0.291	0.25	12.169	0.344	0.136	24.509	0.199	0.135
GAN Uncond	229.106	0.687	0.31	190.955	0.508	0.258	30.398	1.155	0.348	94.96	0.635	0.335
Diff Cond	42.603	0.266	0.094	102.264	0.143	0.166	11.426	0.387	0.137	16.541	0.193	0.123
Diff-CSDI Uncond	172.513	0.485	0.137	265.967	0.058	0.138	47.583	0.5	0.212	100.475	0.342	0.178

Table 1: Realism Comparison.

Average Volume per Price Level. Figure 3 displays the average volume across each of the 10 ask and 10 bid price levels. The real volume exhibits a clear symmetric hump-shaped structure around the best bid and ask prices, with the highest concentration of liquidity at levels 3–6. *GAN Uncond* underestimates volume at nearly all levels. In contrast, *Diff Uncond* and *Diff Cond* closely match the empirical averages, suggesting its ability to reproduce realistic liquidity profiles.

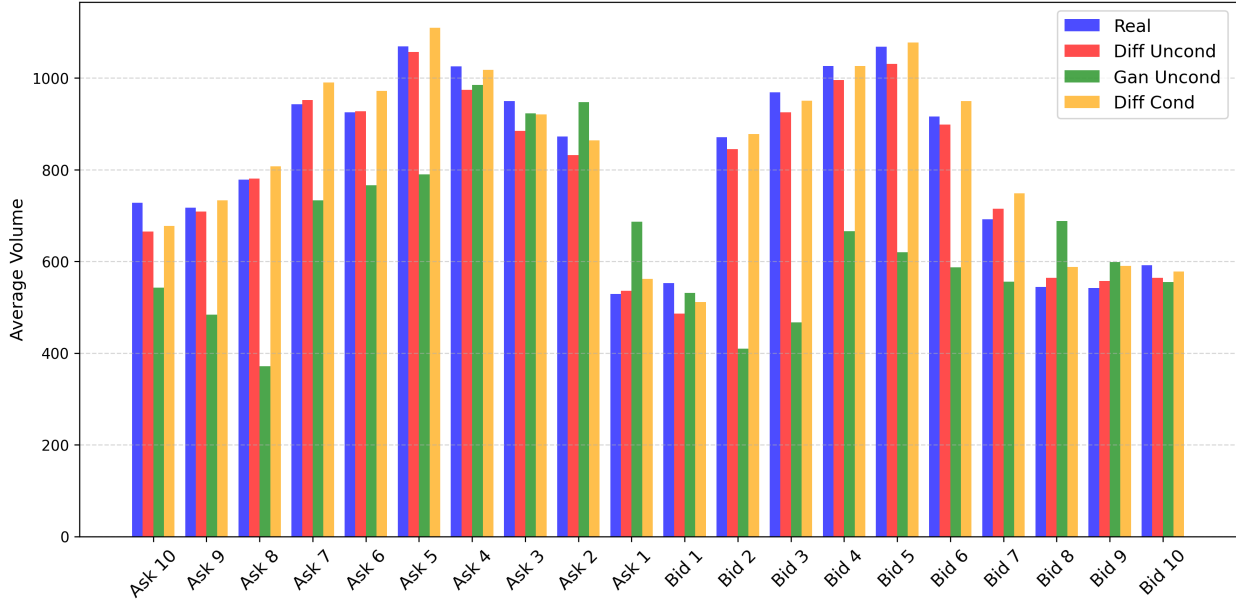


Figure 3: Average Volume per Price Level.

Cross-sectional and Temporal Difference Correlation. Figure 4 shows the cross-sectional volume correlation across 20 price levels (Ask 10 to Bid 10). Compared with *GAN Uncond*, *Diff Uncond* and *Diff Cond* can better capture the spatial structure in the upper left quadrant (Ask 10 to Ask 7) and inter-side interactions (Ask 2 to Ask 6, Bid 2 to Bid 6). Figure 5 is calculated from the first-order differences of the volume snapshots ($\Delta \mathbf{x}_{(i)} = \mathbf{x}_{(i)} - \mathbf{x}_{(i-1)}$). A notable characteristic in the temporal difference correlation structure is the negative correlation at adjacent price levels, which is captured by all three models. However, *Diff Uncond* and *Diff Cond* do better in the upper left quadrant (Ask 10 to Ask 7).

Autocorrelation Decay. Finally, we evaluate the long memory properties of the generated volume series by analyzing autocorrelation decay at each price level, shown in Figure 6 as a log-log plot. In empirical financial time series, volume autocorrelation is known to approximately follow a scaling law Gould et al. [2013]:

$$ACF(l) \sim C \cdot l^{-\gamma}, \quad (10)$$

where $ACF(l)$ denotes the lag- l autocorrelation. The conditional diffusion model closely replicates these dynamics, while the unconditional diffusion model slightly underperforms with faster decay rates. In contrast, the GAN-based approach demonstrates unstable and unrealistic temporal correlations.

To quantitatively evaluate the realism of the generated volume distributions against empirical data, we employ three divergence metrics: Wasserstein distance, Kullback–Leibler (KL) divergence, and Kolmogorov–Smirnov (KS) statistic. The results, summarized in Table 1, consistently indicate that the proposed diffusion-based models substantially outperform the GAN baseline in all four stocks, validating their effectiveness in capturing the empirical volume

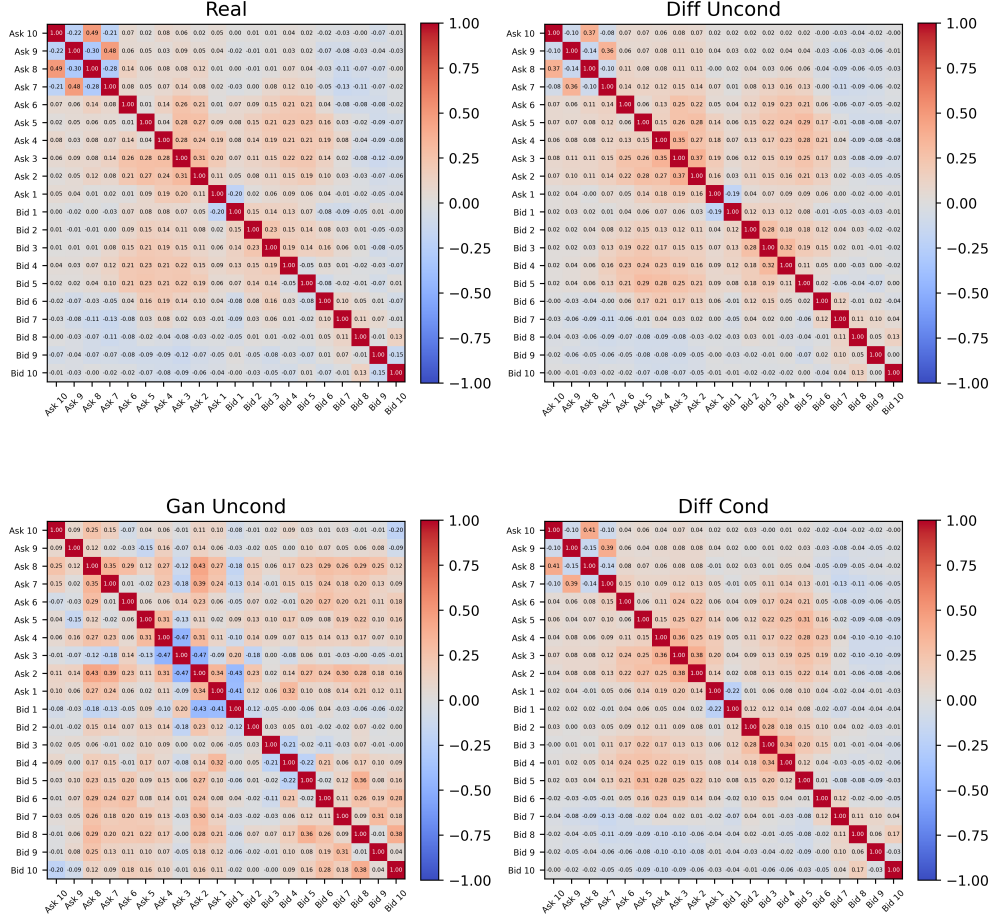


Figure 4: Cross-sectional Volume Correlation.

distribution. Specifically, *Diff Cond* achieves slightly better performance than its unconditional counterpart *Diff Uncond*, highlighting the benefit of incorporating conditioning information. Additionally, *Diff Uncond* outperforms *Diff-CSDI Uncond* model, a diffusion model variant based on the CSDI architecture Tashiro et al. [2021], in almost all cases. This result underscores the superiority of our proposed DiffVolume architecture in modeling limit order book volume distributions.

5.2 Counterfactual Generation under Extreme Liquidity Scenarios

To evaluate the controllability of *Diff Cond* under varying liquidity conditions, we design a counterfactual generation experiment based on liquidity-driven partitioning of the testing dataset. Specifically, we sort all snapshots into five bins (denoted as Bin 1 to Bin 5) based on ascending order of liquidity λ . Bin 1 represents the lowest liquidity regime, whereas Bin 5 corresponds to the highest. The pairwise discrepancies are quantified using the Wasserstein distance, and the results are reported in Table 2.

We first compare *Real_bin* VS *Fake_bin*, where *Real_bin* refers to the subset of real snapshots that fall into each of the five liquidity bins, and *Fake_bin* denotes the corresponding generated samples from *Diff Cond*, conditioned on the past volume history, time of day, and the actual future liquidity value associated with each snapshot in the bin. *Real_all* denotes the entire testing dataset and *Fake_all* denotes the generated dataset by following exact liquidity conditions of *Real_all*. As shown in Table 2, the Wasserstein distances between *Real_bin* and *Fake_bin* are consistently lower than those between *Real_all* and *Fake_bin*. This confirms that *Diff Cond* is highly effective in generating samples closely aligned with the intended liquidity regime.

To further assess the model’s ability to perform counterfactual generation, we fix the past volume trajectory $\mathbf{x}_{(t-L+1:t)}$ and time of day condition τ while altering the target liquidity condition λ to simulate extreme scenarios:

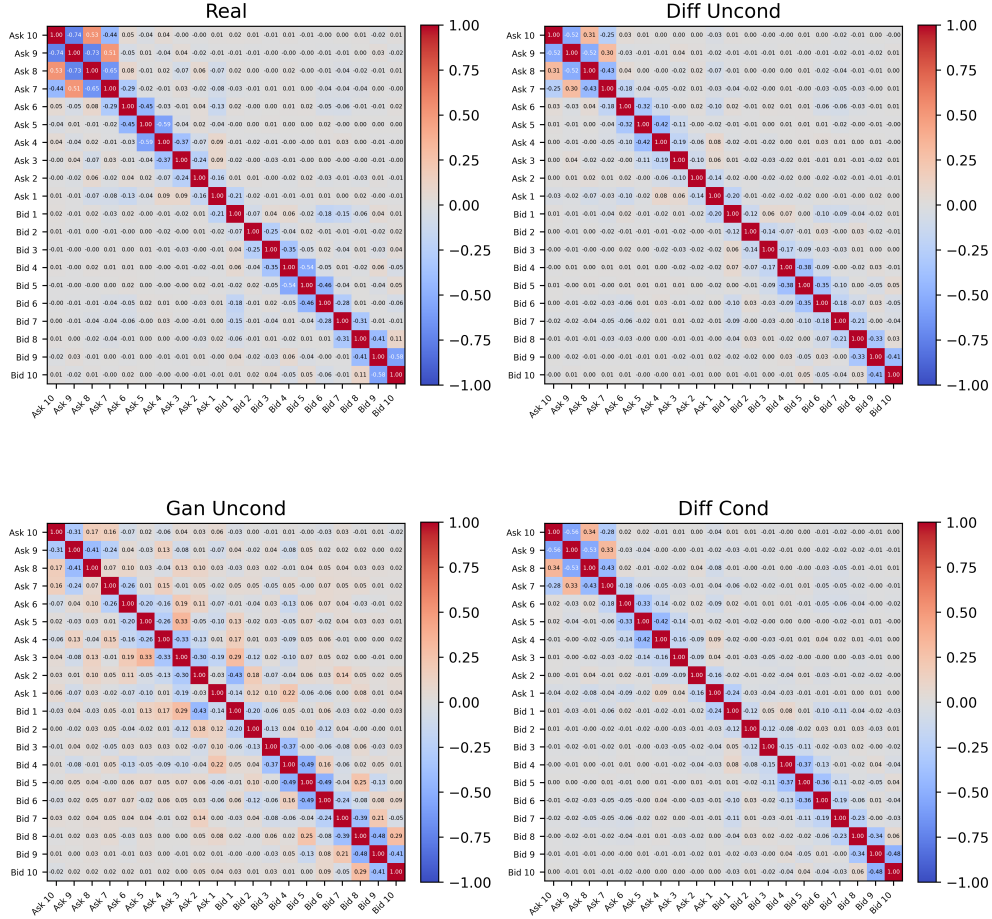


Figure 5: Temporal Difference Volume Correlation.

- Fake_OL_all (Over Liquidity): For every snapshot in the test set, we randomly sample a future liquidity profile from Bin 5 (highest liquidity) and generate new snapshots using the fixed past conditions, time of day and sampled high liquidity.
- Fake_UL_all (Under Liquidity): Similarly, we sample the liquidity condition from Bin 1 (lowest liquidity) while keeping the rest unchanged.

The results show clear trends. The Wasserstein distances between Real_bin and Fake_OL_all decrease progressively from Bin 1 to Bin 5. This indicates that the samples generated under the fixed high liquidity condition resemble more closely those in the high-liquidity bin, validating the model’s ability to simulate high-liquidity scenarios regardless of the original snapshot conditions. Conversely, the distances between Real_bin and Fake_UL_all increase from Bin 1 to Bin 5, suggesting that the low-liquidity condition effectively shifts the output distribution towards the characteristics of low-liquidity environments.

A Case Study on AAPL. We observe that AAPL exhibits an anomalous pattern across bins 3 to 5. Specifically, the Wasserstein distances in Real_bin VS Fake_bin are unexpectedly higher than those in Real_all VS Fake_bin, which is contrary to the trend observed in MU, ADBE, and ZM. Furthermore, in the counterfactual setting (Real_bin VS Fake_OL_all), the expected monotonic decrease in distance from bin 1 to bin 5 is not strictly preserved. Upon examining the underlying data distributions, we find that the liquidity profiles between AAPL’s training and testing datasets differ more substantially than in other stocks. In particular, the average liquidity values across the five bins in the training dataset are $\sim [1.08, 1.36, 1.54, 1.73, 2.07] \times 10^4$, while in the testing dataset they are $\sim [1.54, 1.74, 1.87, 2.00, 2.20] \times 10^4$. Notably, the average liquidity value of bin 3 in the training dataset is approximately equal to that of bin 1 in the testing dataset. This upward shift indicates a distributional drift in liquidity levels between the training and testing phases, which causes the model to misinterpret the intended conditioning during generation when extrapolating to high-liquidity regimes.

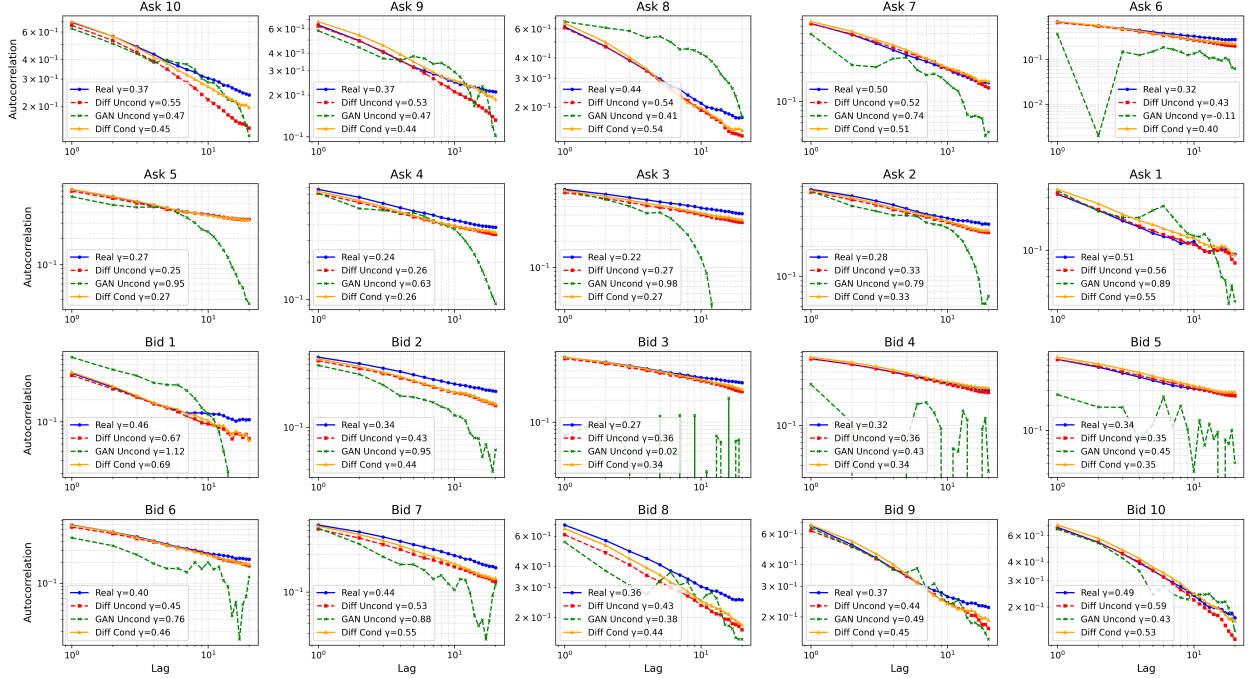


Figure 6: Autocorrelation Decay.

5.3 A Downstream task: Future Liquidity Prediction

To evaluate the utility of synthetic data generated by the proposed *Diff Cond* model, we conduct a downstream task of short-term liquidity forecasting across the four stocks. Specifically, we aim to predict the aggregate LOB volume over the next $Horizon \in \{10, 30\}$ seconds, given a history window of 32 snapshots. Formally, the prediction target at time t is defined as follows:

$$y_t = \sum_{i=1}^H \sum_{j=1}^{20} x_{(t+i)}^j. \quad (11)$$

We employ a LightGBM regressor trained on 27–28 February 2023, and test it on a held-out dataset on March 1, 2023. We compare two training scenarios: *Real* represents that the model is trained solely on the real dataset, while *Real + Synthetic* represents that the model is trained on an augmented dataset combining *Real_all*, *Fake_all*, *Fake_OL_all* and *Fake_UL_all* introduced in Subsection 5.2. Results are reported in Table 3, using Mean Squared Error (MSE), Mean Absolute Error (MAE), R^2 , along with corresponding percentage improvement. By augmenting the training data with generated samples, we achieve consistent improvements in forecasting short-term liquidity. These results demonstrate that *Diff Volume* can also be practically beneficial by providing unseen samples in downstream prediction tasks.

6 Conclusion

In this paper, we propose a novel conditional denoising diffusion probabilistic model for generating future limit order book (LOB) volume snapshots, conditioned on historical order flow, time of day, and optionally target future liquidity levels. Through extensive empirical evaluations, we show that it achieves high realism, closely replicating statistical properties of real market volumes. Second, it supports counterfactual generation, enabling scenario-based simulations under hypothetical liquidity conditions. Third, it proves to be useful for a short-term liquidity prediction task by augmenting real data with synthetic samples. These results highlight the potential of conditional diffusion models as a robust and flexible generative framework for high-frequency financial modeling. Future work includes extending the model to multi-asset settings, joint price-volume generation, and applications to market simulation.

	Liquidity Quintile				
	1	2	3	4	5
MU					
Real_bin VS Fake_bin	41.195	43.223	48.12	46.884	54.666
Real_all VS Fake_bin	163.107	79.411	55.664	108.858	154.762
Real_bin VS Fake_OL_all	306.239	215.215	143.541	142.479	137.262
Real_bin VS Fake_UL_all	120.942	206.558	293.692	357.38	426.005
AAPL					
Real_bin VS Fake_bin	74.576	89.737	105.091	118.66	143.808
Real_all VS Fake_bin	223.924	143.918	98.399	62.155	70.803
Real_bin VS Fake_OL_all	194.573	123.719	115.833	134.759	177.102
Real_bin VS Fake_UL_all	81.01	162.991	225.618	288.545	387.232
ADBE					
Real_bin VS Fake_bin	9.566	10.172	10.817	12.085	16.13
Real_all VS Fake_bin	16.363	10.146	11.207	15.574	26.742
Real_bin VS Fake_OL_all	42.698	31.313	24.686	18.839	14.745
Real_bin VS Fake_UL_all	11.187	8.188	13.509	21.307	36.276
ZM					
Real_bin VS Fake_bin	13.958	15.316	15.024	17.637	26.046
Real_all VS Fake_bin	46.654	20.906	19.718	28.967	65.739
Real_bin VS Fake_OL_all	112.867	84.289	67.306	49.439	27.286
Real_bin VS Fake_UL_all	16.607	26.199	43.166	63.149	102.469

Table 2: Evaluation of Counterfactual Generation

	Horizon = 10			Horizon = 30		
	MSE	MAE	R^2	MSE	MAE	R^2
MU						
Real	162896410	9841	0.7996	1584188284	30962	0.7782
Real + Synthetic	145313593	9590	0.8212	1439704748	30288	0.7985
Percentage	10.79%	2.55%	2.70%	9.12%	2.17%	2.61%
AAPL						
Real	180833992	9831	0.717	1796092385	31156	0.6644
Real + Synthetic	137597830	8892	0.7846	1601342963	29751	0.7008
Percentage	23.91%	9.55%	9.43%	10.84%	4.51%	5.48%
ADBE						
Real	3358510	1464	0.4009	30205360	4422	0.1906
Real + Synthetic	3239457	1428	0.4222	28691234	4228	0.2312
Percentage	3.54%	2.46%	5.31%	5.01%	4.39%	21.30%
ZM						
Real	705321941	23866	-2.8648	7676911350	81013	-4.3042
Real + Synthetic	652072041	22684	-2.573	6195517329	71388	-3.2806
Percentage	7.55%	4.95%	10.19%	19.30%	11.88%	23.78%

Table 3: Liquidity Prediction Results.

Acknowledgements

The authors would like to thank Nikolas Nüsken from the Department of Mathematics at King’s College London for his insightful feedback and helpful suggestions on the manuscript.

References

- Martin D Gould, Mason A Porter, Stacy Williams, Mark McDonald, Daniel J Fenn, and Sam D Howison. Limit order books. *Quantitative Finance*, 13(11):1709–1742, 2013.
- Jean-Philippe Bouchaud, Julius Bonart, Jonathan Donier, and Martin Gould. *Trades, quotes and prices: financial markets under the microscope*. Cambridge University Press, 2018.
- Junyi Li, Xintong Wang, Yaoyang Lin, Arunesh Sinha, and Michael Wellman. Generating realistic stock market order streams. In *Proceedings of the AAAI Conference on Artificial Intelligence*, volume 34, pages 727–734, 2020.
- Andrea Coletta, Matteo Prata, Michele Conti, Emanuele Mercanti, Novella Bartolini, Aymeric Moulin, Svitlana Vyetenko, and Tucker Balch. Towards realistic market simulations: a generative adversarial networks approach. In *Proceedings of the Second ACM International Conference on AI in Finance*, pages 1–9, 2021.

- Peer Nagy, Sascha Frey, Silvia Sapora, Kang Li, Anisoara Calinescu, Stefan Zohren, and Jakob Foerster. Generative ai for end-to-end limit order book modelling: A token-level autoregressive generative model of message flow using a deep state space network. In *Proceedings of the Fourth ACM International Conference on AI in Finance*, pages 91–99, 2023.
- Rama Cont, Mihai Cucuringu, Jonathan Kochems, and Felix Prenzel. Limit order book simulation with generative adversarial networks. *Available at SSRN 4512356*, 2023.
- Luc Bauwens and Nikolaus Hautsch. Modelling financial high frequency data using point processes. In *Handbook of financial time series*, pages 953–979. Springer, 2009.
- Emmanuel Bacry, Iacopo Mastromatteo, and Jean-François Muzy. Hawkes processes in finance. *Market Microstructure and Liquidity*, 1(01):1550005, 2015.
- Vladimir Filimonov and Didier Sornette. Quantifying reflexivity in financial markets: Toward a prediction of flash crashes. *Physical Review E—Statistical, Nonlinear, and Soft Matter Physics*, 85(5):056108, 2012.
- Mark Paddrik, Roy Hayes, Andrew Todd, Steve Yang, Peter Beling, and William Scherer. An agent based model of the e-mini s&p 500 applied to flash crash analysis. In *2012 IEEE conference on computational intelligence for financial engineering & economics (CIFER)*, pages 1–8. IEEE, 2012.
- David Byrd, Maria Hybinette, and Tucker Hybinette Balch. Abides: Towards high-fidelity market simulation for ai research. *arXiv preprint arXiv:1904.12066*, 2019.
- Selim Amrouni, Aymeric Moulin, Jared Vann, Svitlana Vyetrenko, Tucker Balch, and Manuela Veloso. Abides-gym: gym environments for multi-agent discrete event simulation and application to financial markets. In *Proceedings of the Second ACM International Conference on AI in Finance*, pages 1–9, 2021.
- Tucker Hybinette Balch, Mahmoud Mahfouz, Joshua Lockhart, Maria Hybinette, and David Byrd. How to evaluate trading strategies: Single agent market replay or multiple agent interactive simulation? *arXiv preprint arXiv:1906.12010*, 2019.
- Hanna Hultin, Henrik Hult, Alexandre Proutiere, Samuel Samama, and Ala Tarighati. A generative model of a limit order book using recurrent neural networks. *Quantitative Finance*, 23(6):931–958, 2023.
- Jascha Sohl-Dickstein, Eric Weiss, Niru Maheswaranathan, and Surya Ganguli. Deep unsupervised learning using nonequilibrium thermodynamics. In *International conference on machine learning*, pages 2256–2265. PMLR, 2015.
- Jonathan Ho, Ajay Jain, and Pieter Abbeel. Denoising diffusion probabilistic models. *Advances in neural information processing systems*, 33:6840–6851, 2020.
- Alexander Quinn Nichol and Prafulla Dhariwal. Improved denoising diffusion probabilistic models. In *International conference on machine learning*, pages 8162–8171. PMLR, 2021.
- Jiaming Song, Chenlin Meng, and Stefano Ermon. Denoising diffusion implicit models. *International Conference on Learning Representations*, 2021a.
- Pascal Vincent. A connection between score matching and denoising autoencoders. *Neural computation*, 23(7):1661–1674, 2011.
- Yang Song and Stefano Ermon. Generative modeling by estimating gradients of the data distribution. *Advances in neural information processing systems*, 32, 2019.
- Yang Song, Jascha Sohl-Dickstein, Diederik P Kingma, Abhishek Kumar, Stefano Ermon, and Ben Poole. Score-based generative modeling through stochastic differential equations. *International Conference on Learning Representations*, 2021b.
- Tero Karras, Miika Aittala, Timo Aila, and Samuli Laine. Elucidating the design space of diffusion-based generative models. *Advances in Neural Information Processing Systems*, 35:26565–26577, 2022.
- Kelvin JL Koa, Yunshan Ma, Ritchie Ng, and Tat-Seng Chua. Diffusion variational autoencoder for tackling stochasticity in multi-step regression stock price prediction. In *Proceedings of the 32nd ACM International Conference on Information and Knowledge Management*, pages 1087–1096, 2023.
- Zhuohan Wang and Carmine Ventre. A financial time series denoiser based on diffusion models. In *Proceedings of the 5th ACM International Conference on AI in Finance*, pages 72–80, 2024.
- Calvin Luo. Understanding diffusion models: A unified perspective. *arXiv preprint arXiv:2208.11970*, 2022.
- Stanley Chan et al. Tutorial on diffusion models for imaging and vision. *Foundations and Trends® in Computer Graphics and Vision*, 16(4):322–471, 2024.
- Brian DO Anderson. Reverse-time diffusion equation models. *Stochastic Processes and their Applications*, 12(3):313–326, 1982.

- Jonathan Ho and Tim Salimans. Classifier-free diffusion guidance. *NeurIPS 2021 Workshop on Deep Generative Models and Downstream Applications*, 2021.
- Ashish Vaswani, Noam Shazeer, Niki Parmar, Jakob Uszkoreit, Llion Jones, Aidan N Gomez, Łukasz Kaiser, and Illia Polosukhin. Attention is all you need. *Advances in neural information processing systems*, 30, 2017.
- Ethan Perez, Florian Strub, Harm De Vries, Vincent Dumoulin, and Aaron Courville. Film: Visual reasoning with a general conditioning layer. In *Proceedings of the AAAI conference on artificial intelligence*, volume 32, 2018.
- Aäron van den Oord, Sander Dieleman, Heiga Zen, Karen Simonyan, Oriol Vinyals, Alex Graves, Nal Kalchbrenner, Andrew W. Senior, and Koray Kavukcuoglu. WaveNet: A Generative Model for Raw Audio. In *Proceedings of the 9th ISCA Speech Synthesis Workshop (SSW)*, pages 125–131, 2016.
- Ruihong Huang and Tomas Polak. Lobster: Limit order book reconstruction system. *Available at SSRN 1977207*, 2011.
- Antonio Briola, Silvia Bartolucci, and Tomaso Aste. Hlob–information persistence and structure in limit order books. *Expert Systems with Applications*, 266:126078, 2025.
- Ian Goodfellow, Yoshua Bengio, Aaron Courville, and Yoshua Bengio. *Deep learning*, volume 1. MIT press Cambridge, 2016.
- Diederik P. Kingma and Jimmy Ba. Adam: A method for stochastic optimization. *International Conference on Learning Representations*, 2015.
- Yusuke Tashiro, Jiaming Song, Yang Song, and Stefano Ermon. Csd: Conditional score-based diffusion models for probabilistic time series imputation. *Advances in Neural Information Processing Systems*, 34:24804–24816, 2021.